fractal and fractional

MDPI

Article

Experimental Investigation of the Fractal-Permeability Properties of Locally Fractured Coal Bodies around Gas Extraction Boreholes

Mingkun Pang [1,2,3], Hongyu Pan [1,3,*], Shipeng Zhu [1], Yao Zhang [1] and Tianjun Zhang [1]

[1] College of Safety Science and Engineering, Xi'an University of Science and Technology, Xi'an 710054, China; pang05016@126.com (M.P.)
[2] College of Energy, Xi'an University of Science and Technology, Xi'an 710054, China
[3] Key Laboratory of Western Mine Exploitation and Hazard Prevention of the Ministry of Education, Xi'an 710054, China
* Correspondence: 19120089022@stu.xust.cn; Tel.: +86-13201744223

Abstract: To investigate the permeability characteristics in the in-situ fractured coal body around the perimeter of gas extraction boreholes, the steady-state permeability of fractured coal bodies with different gradations was tested using the fractured rock permeability test system. By controlling the axial displacement and permeability pressure, the permeability parameters were obtained under different porosities. The interactions between the permeability parameters and the process of permeability destabilisation are discussed. The results show that the permeability characteristics of the broken coal body obey the Forchheimer relationship: As the axial displacement increases, the permeability resistance of the fluid increases and the non-Darcy property of the sample becomes more significant. With the decrease in the porosity of the sample and the increase in the power index n, the permeability k decreases and the non-Darcy factor β increases. The final fractal structure of the sample will be changed by particle fragmentation and migration during the loading process of the sample with different levels, and the internal pore structure of the sample will further affect the penetration of the penetration channel. A critical characteristic value for the seepage instability in broken coal bodies is given, and an expression for determining the seepage instability by permeability and non-Darcy factors is proposed. The results indicate that a negative non-Darcy factor is not a necessary condition for permeability instability, and the critical Reynolds number for the permeability instability in broken coal bodies was determined from the perspective of the Reynolds number. The conclusions of this study can provide theoretical support for the theoretical study of permeability and the permeability of pre-smoking coal seams.

Keywords: gas extraction; fractal characteristics; fractured coal bodies; non-Darcy flow; Reynolds number; flow pattern distribution

Citation: Pang, M.; Pan, H.; Zhu, S.; Zhang, Y.; Zhang, T. Experimental Investigation of the Fractal-Permeability Properties of Locally Fractured Coal Bodies around Gas Extraction Boreholes. *Fractal Fract.* **2023**, *7*, 574. https://doi.org/10.3390/fractalfract7080574

Academic Editor: Norbert Herencsar

Received: 1 June 2023
Revised: 11 July 2023
Accepted: 24 July 2023
Published: 25 July 2023

1. Introduction

Gas extraction is the basis of mine gas management [1]. Drill holes can be divided into an unloading zone area, a stress concentration zone area, and an original stress zone area according to the stress characteristics along the drilling direction [2]. In the unloading zone area, the stress exceeds the strength of the coal body, causing the coal body to be fractured while remaining in its original position, forming a special structure coal body, i.e., an in-situ fractured coal body [3,4]. In the drilling and extraction process, due to the presence of the special structure of this in-situ fractured coal body, it is important to investigate the evolution of its permeability parameters and the seepage instability characteristics, providing an important theoretical reference value for the gas transportation behaviour around the hole and the improvement of gas extraction efficiency. However, influenced by the high permeability pressure downhole, the gas continuously moves towards the interior

of the borehole under the pressure of the peripheral coal body, resulting in deformation and damage phenomena such as erosion, opening, extension, and penetration, with severe deformation of the pore structure, leading to strong non-linear characteristics of seepage flow [5,6].

The in-situ crushed coal body around the perimeter of a borehole is composed of crushed coal bodies that are stuck together to form different grain sizes [7,8]. A series of studies have also been conducted by many experts to investigate the influence of the structure of perforated crushed coal bodies on their permeability properties. By using NMR techniques and non-Darcy models, Liu et al. [9] and Ma et al. [10] quantified the pore structure and hydraulic properties of the fractured rock mass and obtained the flow characteristics of non-Darcy flow in the rock mass, showing that the seepage in the rock mass no longer follows Darcy's law but follows the Forchheimer equation. Based on seepage tests, Li et al. [11] established a non-linear kinetic equation for seepage in fractured rocks, finding the equilibrium state in which the seepage system in fractured rocks tends to the compacted state and analysing the stability of the equilibrium state. Dusabemariya et al. [12] concluded that the non-Darcy flow characteristics of fractured rocks are related to the porosity of the fractured rock. Using mechanical systems and specially developed devices, Wu et al. [13] and Lv et al. [14] measured the seepage characteristics of fractured sandstones during the process of non-Darcy seepage and calculated the permeability and non-Darcy seepage β factor using the steady-state seepage method. Wang et al. [15] investigated the seepage characteristics of fractured rocks with different grain sizes and porosities. Steady-state percolation tests were conducted on fractured rocks of five grain sizes. By binary fitting of the experimental data, Liu et al. [16] obtained the relationship between non-Darcy permeability parameters and porosity and grain size. By studying the effects of different porosity and grain size coupling mechanisms on the seepage characteristics of fractured rocks, Qiu et al. [17] found that the relationship between permeability and both porosity and grain size could be expressed as an exponential function.

In order to more accurately study the permeability characteristics of an in-situ fractured coal body, a porous medium, researchers used the fractal theory to describe the microstructure of porous media [18–20]. Based on the fractal theory and Talbot classification theory, to prepare test samples, Li et al. [21] investigated the seepage evolution of fractured rock bodies under triaxial stress using a triaxial seepage test apparatus. Karacan et al. [22] proposed a method to predict the permeability and porosity of coal bodies in mining areas based on the fractal scale and the principle of fluid flow in porous media. A laboratory compaction test system was used to perform loading tests on crushed rocks with different particle sizes. Based on the crushing characteristics and particle size distribution of the samples, Kong et al. [23] discussed the fractal behaviour of particle sizes and the energy dissipation during the loading of fractal scale characteristics to provide a reference for further analysis of their permeability. Based on the experiments and combined with fractal theory, Sarkar et al. [24] proposed a fractal-dimension-based method of calculation for the rock-crushing particle size model. Fractal theory was used to provide a better analysis of the particle size characteristics of negatively crushed rocks, and Lei et al. [25] characterised the permeability evolution. Using this model to fully couple coal deformation with gas flow, Liu et al. [26] developed a fractal permeability model and found that the pore fractal dimension varied with the effective stress through porosity and that the macroscopic permeability of coal was proportional to the fractal dimension. Combining the structural fractal dimension calculated by the incremental fractal constitutive method, Liu et al. [27] concluded that the fractal dimension of the pore structure and volume can quantitatively describe the specific surface area of porous media and is proportional to the specific surface area. As the fractal dimension of the structure increases, the resistance to fluid flow increases and the theoretical permeability decreases. Using fractal geometry theory and related methods to simulate the pore curvature and roughness of coal bodies, Xiao et al. [28] established a model relating the permeability of porous media to structural

parameters such as the pore area fractal dimension, the pore curvature fractal dimension, and so on.

Several results have been obtained from the above studies on the permeability characteristics of crushed coal bodies, but less research has been conducted on the interaction between the permeability parameters of crushed coal bodies and seepage stability during the permeation process. In the present work, an in-situ percolation test on the crushed coal body around different particle sizes and different axial displacement boreholes was designed to obtain the deformation and seepage instability of the crushed coal body. The evolution of the porosity and permeability was then determined based on the permeability parameters measured in the test. Finally, the relationships between the Reynolds number, osmotic pressure, and seepage stability during infiltration were investigated.

2. Theory

During the extraction of gas resources, the stress concentration around the borehole is likely to cause damage to the coal body, further forming many pores and fracture networks; these "ring" pores and fractures are called the fracture field of the borehole. The gas flow in the coal body around the borehole enters the borehole through the fissure field, which is a necessary channel for the flow of extracted gas. Damage to the coal around the borehole is mainly in the form of dispersion and fractures, and the fracture network on the inner wall of the borehole is also characterised by fissure alignment and fissure size. A realistic view of coal damage around a borehole disturbed by stress concentration is displayed in Figure 1.

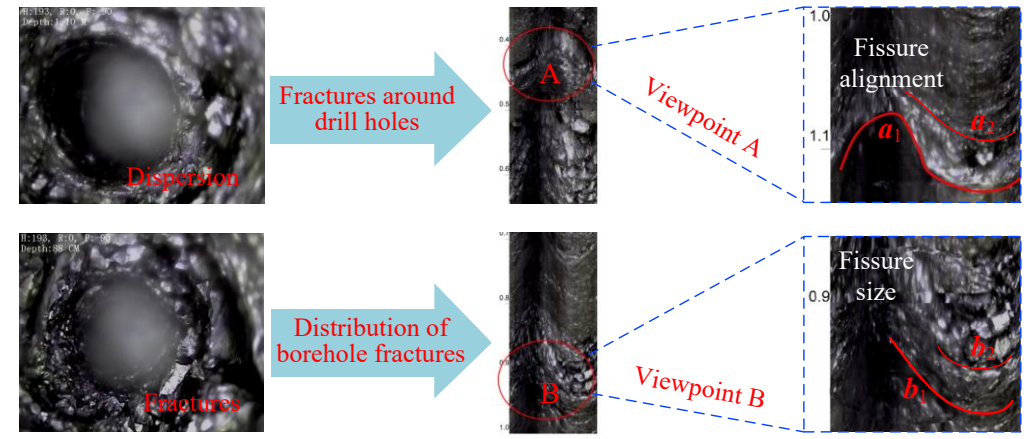

Figure 1. Realistic view of coal damage around a borehole disturbed by stress concentration.

The current research into gas flow within the fracture field of the coal body around the borehole belongs to the field of dual medium flow, where the pore and fracture structures around the borehole are considered as two separate permeable media [29]. The flow process can also be divided into three main stages:

① Gas in the coal body around the borehole enters the pore space under the effect of concentration difference, forming the gas diffusion phenomenon; following Fick's law of diffusion, the flow equation is $J = -D\left(\frac{\partial C}{\partial X}\right)$.

② Gas in the pore space enters the fissure under the action of pore pressure difference, forming the gas infiltration phenomenon; following Darcy's law, the flow equation is $v = -\frac{k_D}{\mu}\frac{\partial p}{\partial x}$.

③ Gas in the fissure converges into the extraction borehole under the action of the negative extraction pressure, forming the sinking gas phenomenon.

3. Materials and Methods

To study the flow pattern of gas in the fracture field around the extraction borehole, coal samples from high-gas mines were selected and triaxial seepage tests on fractured coal bodies were conducted using the grading theory to prepare multiple sets of samples with a certain initial porosity and considering different stresses and different permeability pressures.

3.1. Materials

3.1.1. Research Background

The sample was taken from Shaanxi Huangling No. 2 Coal Mine Co., Ltd. (Yanan, China) with a shaft area of 351.94 km^2, resource reserves of 970 Mt, recoverable reserves of 640 Mt, and a mine service life of 70 years. Engineers used the extraction ventilation method, with a central parallel ventilation system, with the main and secondary risers feeding the mine and the west return riser returning the mine. The main mining seam 3# coal, with a thickness of 6.34 m, has an inclination of 0° to −5°, with an average inclination of +0.5° in the direction of the N1101 tape chute cutting. The 3# coal seam is black, lumpy, locally powdery, and shiny. Yuwu Coal Company was designed as a high-gas mine with a gas content of 10.0496 m^3/t. The absolute gas outflow from the mine in the last three years is 294.38 m^3/min and the relative gas outflow is 21.08 m^3/t. The old top of the 3# coal seam is sandy mudstone, 9.78 m. The direct top is mudstone, 2.25 m. The old bottom is sandy mudstone, 8.4 m. The direct bottom is siltstone—fine-grained sandstone, 6.10 m.

3.1.2. Material Preparation

The gas extraction borehole is affected by stress concentration, which will produce a "ring" rupture area, where the perimeter of the borehole is mainly composed of fractured coal. The fractured coal body, as the main channel of gas influx into the borehole, has a high porosity and a high permeability. The test sample was taken from Shaanxi Huangling No. 2 coal mine, and its bulk density was found to be 1566 kg/m^3 by coring. Considering that, in engineering practice, the crushed coal body around the hole consists of multiple scale particle sizes, the crushed coal was sieved into four particle size intervals of 2.5~5 mm, 5~10 mm, 10~15 mm, and 15~20 mm using a sorting sieve [30]. In addition, to overcome the dimensional catastrophe, the mass fraction of particles within each particle size interval was calculated according to Talbot's continuous grading theory, i.e.,

$$P = \left(\frac{d}{D}\right)^n \times 100\% \quad (1)$$

where P is the percentage of a particle size less than diameter d; d is the current particle size of the sample, mm; D denotes the largest particle size in the composition of the sample, mm; and n represents the Talbot power index.

According to the size of the test permeameter, the total mass of a single group of samples is 800 g, and four groups of samples with a Talbot power index of 0.2, 0.4, 0.6, and 0.8 are taken to form different grading structures, and Equation (1) can be calculated to obtain the percentage of each particle size interval at different Talbot power indices, as shown in Figure 2, and the preparation of four sets of samples of crushed coal bodies is shown in Figure 3.

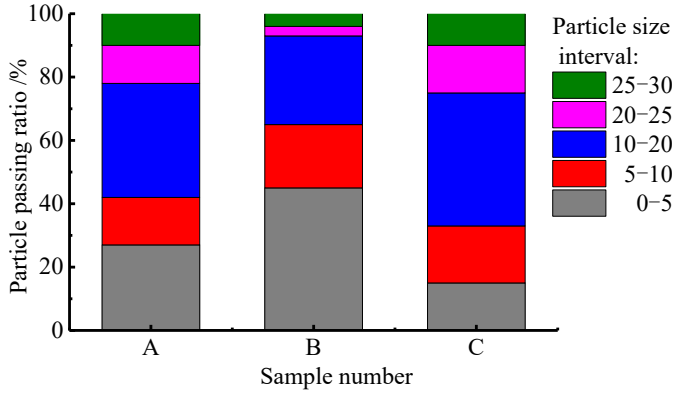

Figure 2. Distribution of the four particle sizes of crushed coal bodies.

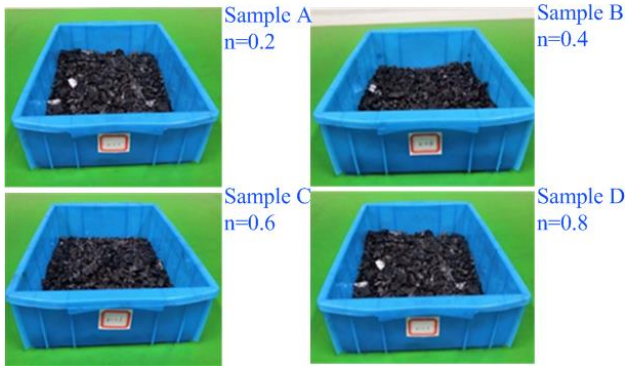

Figure 3. Preparation of four sets of samples of crushed coal bodies.

3.2. Methodologies

3.2.1. Experiment Design

The permeation test of the crushed coal body around the borehole was conducted by the steady-state permeation method, and the magnitude of the permeation pressure was easy to control during steady-state permeation. Meanwhile, the porosity of the sample can be controlled by controlling the axial displacement, suggesting that the porosity of the sample could be controlled, and the gradient of the permeation pressure to which the sample was subjected could also be controlled to remain consistent; therefore, axial displacement control was adopted in the present research [31].

The porosity of the crushed coal body at each stage can be determined from the axial displacement S at that stage, as given by the following:

$$\phi = 1 - \frac{m_0}{\rho_0 A(H - S)} \tag{2}$$

where m_0 is the total mass of the crushed coal sample, kg; ρ_0 is the density of the coal sample, kg/m^3; A stands for the internal bottom area of the cylinder, m^2; H stands for the initial height of the sample, m; and S represents the axial control displacement, m.

The percolation rate can be calculated from the flow rate as follows:

$$V = \frac{Q}{A} \tag{3}$$

where V is the percolation velocity, m/s; Q is the flow rate through the sample, m^3/s; and A is the cross-sectional area of the sample, m^2.

Let the height of the sample at a certain stage be H_s, the osmotic pressure at the inlet of the permeameter be the set value P_1, and, since the outlet end is together with the

atmosphere, the osmotic pressure at the outlet end $P_2 = 0$. Therefore, the osmotic pressure gradient G_p in the sample can be calculated as [32] follows:

$$G_p = \frac{P_2 - P_1}{H_s} = -\frac{P_1}{H_s} \tag{4}$$

Existing research shows that [33] the seepage behaviour in the fractured coal body obeys the Forchheimer relationship, and herein, the steady-state permeability method was adopted. The acceleration of the fluid is 0; therefore, the Forchheimer equation can be simplified to the following:

$$-G_p = \frac{\mu}{k}V + \beta\rho V^2 \tag{5}$$

where k is the permeability and β is the non-Darcy factor.

According to the osmotic pressure gradient and the corresponding seepage velocity during the test, the permeability k and the non-Darcy flow β factor can be fitted according to Equation (5).

3.2.2. Experimental Equipment

The permeation test of the crushed coal body around the borehole was conducted using the crushed rock permeation test system, which mainly consists of a pressure machine, a crushed rock permeation meter, a permeation pressure control pump, a data recording system, pipelines, and metering instrument accessories. The crushed coal body triaxial permeation test system is illustrated in Figure 4.

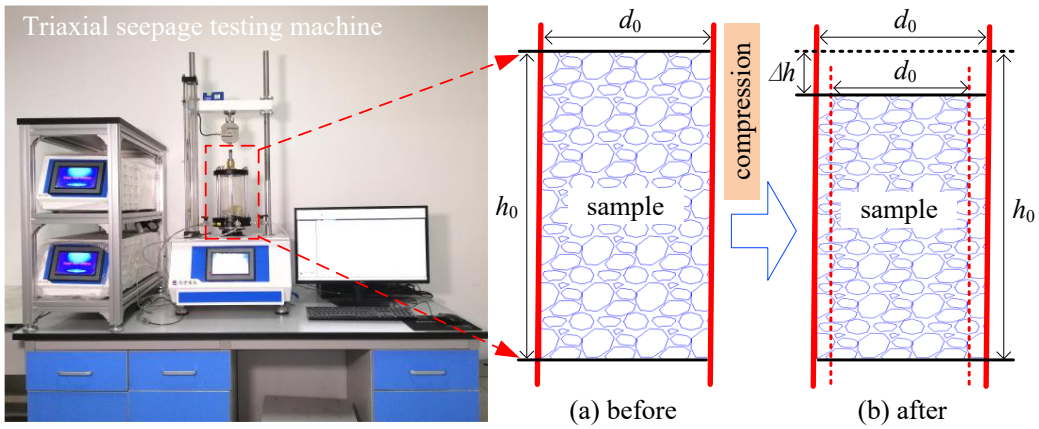

Figure 4. Triaxial seepage test system for crushed coal bodies.

To obtain the permeation characteristics of the crushed coal body at different axial displacements, four stages of a displacement of 3, 6, 9, and 12 mm were applied axially, and four stages of a permeation pressure of 0.5, 1.0, 1.5, and 2.0 MPa were applied under each stage of axial displacement. To acquire the seepage data of the crushed coal samples under different pressure gradients, during the test, the data-logging system recorded the axial pressure F and axial displacement S applied by the press, as well as the permeation pressure P and the flow rate Q through the specimen during each stage of permeation in real time and saved them.

3.2.3. Experimental Procedure

During the test, the axial pressure and displacement of the crushed coal body could be adjusted by the press, and when the predetermined value was reached, the permeation pump could be turned on to control the size of the permeation pressure, and the steady-state permeation of the crushed coal body under different permeation pressures could be tested. The specific test procedure is as follows:

- Load the crushed coal sample into the penetrometer and complete the assembly of the system according to the schematic diagram. Record the initial height of the specimen and set the pressure and displacement to 0;
- Control the press to apply axial pressure and control the pressure (displacement) to a predetermined value;
- Turn on the osmotic pressure control pump to adjust to a predetermined osmotic pressure level for the permeation test, which needs to be maintained for more than 15 s at each level of osmotic pressure, and record the flow and pressure values of the import and export during the permeation process;
- Turn off the osmotic pressure control pump, remove the pressure to take out the specimen, clean the permeameter, and conduct the next set of tests according to experimental needs;
- To reduce the test error, for each group of specimens, repeat the test three times. The test results consist of the average of the three tests;
- Through use of the aforementioned test method, the permeability characteristics of the crushed coal body can be measured at different axial pressures and different porosities.

After each completed set of measurements on one specimen had been recorded, its stress-strain data were obtained through the computer data acquisition system, and then the previous steps were repeated for the other specimens, and each set of data could be recorded until the test was completed.

4. Results and Discussion

To study the permeability characteristics of the crushed coal grains around the extraction borehole, a fractal-percolation test study was conducted independently to determine the distribution of permeability velocity at various levels of displacement and to clarify the relationship between the permeability parameters of the crushed coal body. Based on the deformation characteristics of the permeable skeleton of the crushed coal body, the process of seepage destabilisation of the crushed coal body around the extraction borehole is then discussed.

4.1. Permeation Velocity Distribution Pattern at Each Level of Displacement

The seepage velocity distribution of the fractured coal body at different degrees of compression needs to be further investigated. Four axial displacements of F_1, F_2, F_3, and F_4 (3 mm, 6 mm, 9 mm, and 12 mm) were set in the test, and seepage pressures of 2.0 MPa, 4.0 MPa, 8.0 MPa, and 12.0 MPa were selected for the infiltration test study. By collating the test results, the seepage velocity data at different axial displacements and different osmotic pressures could be obtained, and the relationship between the seepage velocity and the osmotic pressure gradient at different axial displacements were plotted according to the data (Figure 5).

As can be seen from Figure 5, as the absolute value of the osmotic pressure gradient increases, the flow rate of the fluid increases (albeit to a lesser extent). At the beginning of loading, a trend of increasing flow velocity is evident, while with the increase in displacement, the rate of increase in the flow velocity decreases significantly. This is because as the axial displacement increases, the pore channels in the specimen are gradually compacted and the particles are fractured under pressure, causing the structure of the specimen to adjust and causing blockage or dimensional changes in the fluid channels of the specimen. The flow of the fluid will bear small particle sizes to the outlet from the specimen, and this transport process will also lead to changes in the flow path and local pore structure changes. The combination of these factors will affect the overall percolation velocity, causing a decrease in the increase in percolation velocity and causing a non-linear increase.

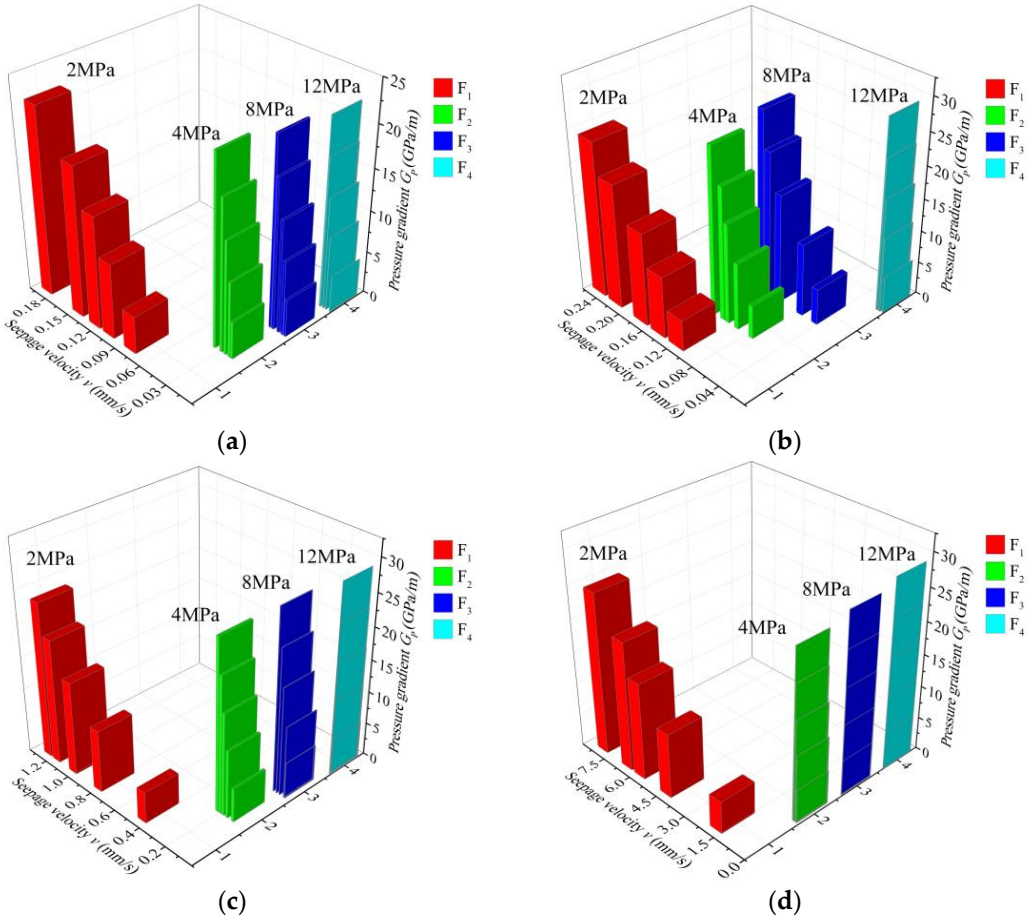

Figure 5. Relationship between percolation rate and pore pressure gradient for each group of specimens. (**a**) Skeleton dense structure fractured sample; (**b**) suspended dense structure fractured sample; (**c**) skeleton void structure fractured sample; (**d**) contrasting structural crushing samples.

The fitted curves of the permeation velocity versus the permeation pressure gradient are also consistent with non-linearity through the different axial displacement stages, i.e., the permeation process in the fractured coal body exhibits non-Darcy percolation. An analysis of the fitted functions reveals that the fitted results for the permeability velocity and osmotic pressure gradient are consistent with the Forchheimer equation and are consistent for different axial displacements. At the same time, the power index, which characterises the grading structure, exerts a certain influence on the permeation of the specimens, and the deviation from Darcy's law is more significant when the power index is 0.2 than 0.8. This is because with a lower power index, the proportion of small- and medium-grain-size intervals in the crushed coal body will increase, and the pore structure will be denser, making non-Darcian phenomena more obvious. In summary, it can be concluded that the permeability characteristics of fractured coal bodies show non-Darcian behaviour and obey the Forchheimer relationship.

4.2. Relationships between Permeability Parameters of Crushed Coal Bodies

The pore structure characteristics of the crushed coal specimen are important factors affecting the permeability of the specimen, such as the number of pores, individual pore size, pore distribution characteristics, the degree of pore connectivity, etc. Porosity is used as the main parameter to characterise the pore characteristics, and the effect of porosity on permeability can be obtained by studying the four sets of test results, as shown in Figure 6.

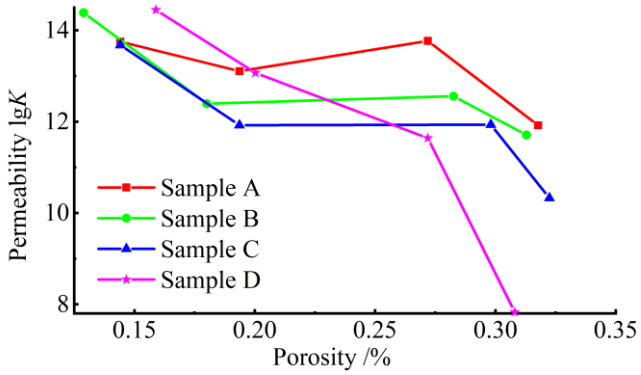

Figure 6. The permeability and porosity of crushed coal samples with different grading structures.

As illustrated in Figure 6, the permeability of the crushed coal body increases as the porosity increases (albeit to a decreasing extent because when the porosity is larger, the internal pore penetration is enhanced, the flow rate and flow rate through the specimen changes less, and the permeability of the specimen changes less, while when the porosity of the specimen is smaller, the internal pore structure of the specimen is relatively dense, and the permeability of different grading structures shows greater variability, the larger the power index n, the greater the permeability of the specimen, which further illustrates that the permeability of the crushed coal body is not only related to the porosity but is also related to the power index n).

The relationship between the porosity and non-Darcy factor is given in Figure 7, which shows that as the porosity increases the non-Darcy factor decreases, and when porosity is low, the non-Darcy factor of the specimen is larger, indicating that the lower the porosity, the lower the penetration of the internal channels of the specimen, leading to a high resistance to percolation channels, leading to a more pronounced non-Darcy phenomenon in the fractured coal body. However, the curve exhibits local undulations, while the non-Darcy factor of the specimen decreases as the power index n increases. The reasons for these phenomena are closely related to the dislocation, fragmentation, and dislodgement of particles in porous media and depend on the reorganisation of the specimen particles and the evolution of the internal pore structure. Seepage instability occurs when the non-Darcy factor is negative. The absence of a negative non-Darcy factor in this experiment does not mean that seepage instability did not occur during the test, and the subsequent instability characterisation also indicates that seepage instability did occur during the test.

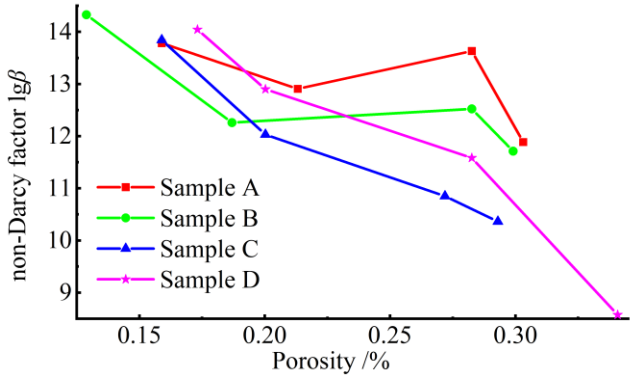

Figure 7. Non-Darcy factors and porosity of crushed coal samples with different grading structures.

The combined effect of porosity on the permeability and non-Darcy factor shows that a decrease in the porosity leads to multiple closed permeable channels, resulting in a sharp decrease in permeability k. Meanwhile, the difference in the power index n of the gradation leads to different permeability resistances of the specimens, triggering changes in

the β values; therefore, further consideration of the relationship between the permeability and non-Darcy factors is shown in Figure 8.

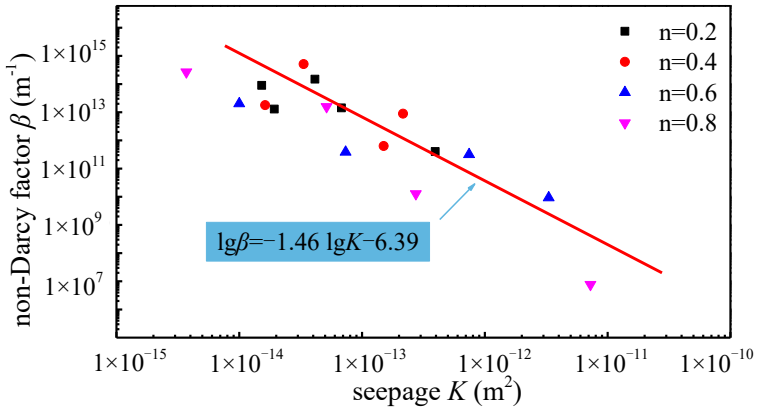

Figure 8. Non-Darcy factors and permeability of fractured coal samples with different grading structures.

Figure 8 shows that the non-Darcy factor of the specimen decreases as the permeability increases, which also indicates that when the permeability of the specimen is greater, the specimen allows more fluid to pass through and the resistance to fluid is less. In contrast, when the permeability is small, the pore structure of the specimen is denser and the resistance to fluid flow is larger, and the non-Darcy factor is more pronounced; the variation pattern shows consistency at different power indices n.

4.3. Deformation Characteristics of the Permeable Skeleton of a Fractured Coal Body

As the axial displacement and porosity change, the permeability characteristics of the specimen will be affected. The reason for this is that with the increase in the axial displacement, the permeability skeleton of the specimen is deformed, and an adjustment of the pore structure occurs. In the initial small displacement stage, due to the large porosity of the crushed coal specimen, the bearing capacity of the specimen's skeleton is weak at this time, and the stress required to reach the predetermined displacement is small, and the deformation is mainly attributed to the relatively high coal content in the large particle size zone of the specimen at this time, and the contact between the particles is in the form of point-to-point and point-to-face contact, readily generating local stress concentrations, followed by a rupture and crushing of the particles. With the continued control of displacement, in the previous stage of the specimen, there was a certain degree of compaction and structural adjustment, and the bearing capacity of the specimen's skeleton increased. The stage after the loading process of the mutual grinding particles' particle shape becomes relatively uniform; this process of particle breakage is then diminished. As the load is increased, the contact between the particles becomes dense and the small particles fill the gaps between the large particles to form a stable pressure-bearing structure, and the force required to produce the required deformation increases significantly. The deformation of the specimen affects the number and connectivity of the permeation channels, increasing the resistance to the fluid and changing its flow regime.

In the Forchheimer formula, the viscous resistance can be expressed as a linear component of the permeation velocity and the inertial resistance as a non-linear component to obtain the relationship between the viscous resistance, the proportion of inertial resistance, and the permeation velocity, as shown in Figure 9.

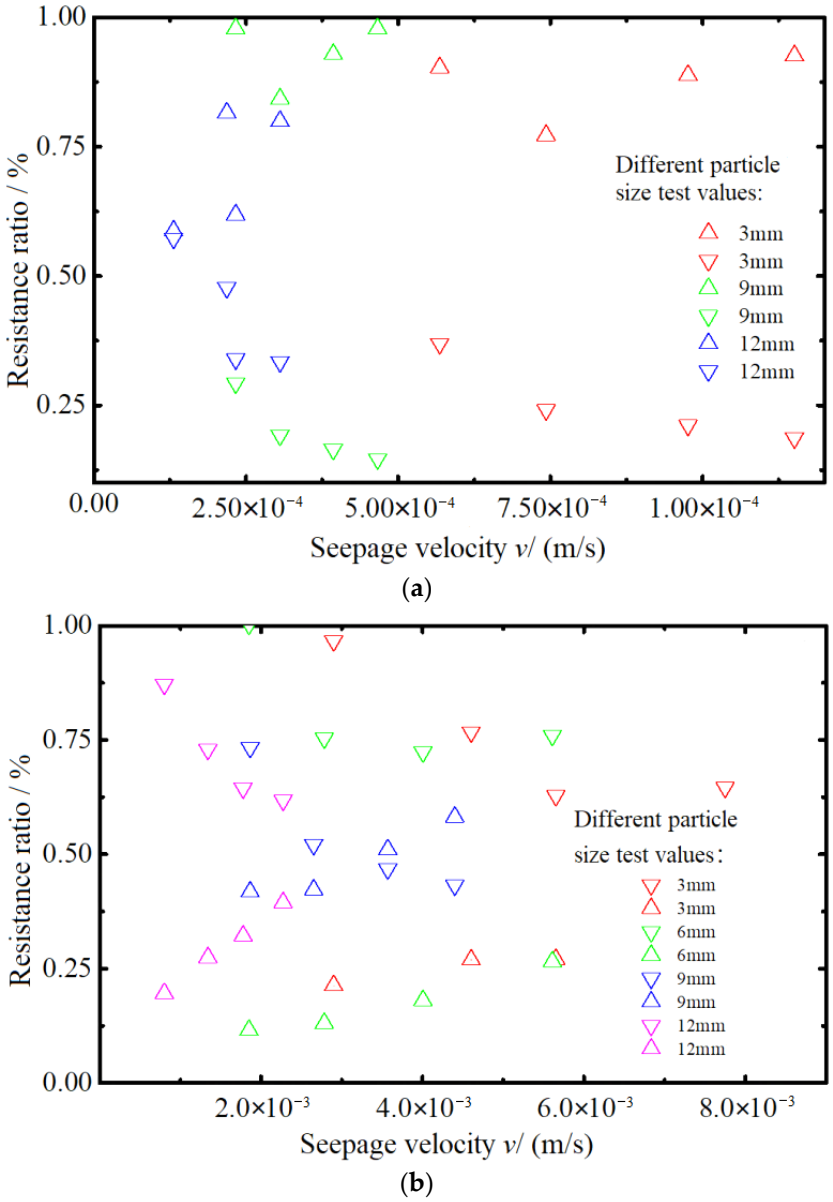

Figure 9. Specific gravity and flow rate of crushed samples from suspended dense structures and comparison groups. (**a**) Suspended dense structure crushing samples; (**b**) contrasting structural crushing samples.

As shown in Figure 9, the specific gravity of the force applied to the fluid during infiltration is always greater than the inertial force resistance, while the specific gravity of the viscous force resistance decreases and the specific gravity of the inertial force resistance increases as the infiltration velocity increases. This is because the viscous resistance and inertial resistance increase although the fluid increases at six years of age, but the rate of increase in the inertial resistance is greater than the rate of increase in the viscous force resistance. The sum of the two resistances is the osmotic pressure gradient, and when the non-linear specific gravity exceeds 0.5, the non-Darcy flow dominates, i.e., the Forchheimer equation better describes the osmotic state, in good agreement with the fitted relationship between the osmotic velocity and the osmotic pressure gradient.

4.4. A Discussion of Seepage Destabilisation Processes in Fractured Coal Bodies

4.4.1. Derivation of the Seepage Instability Conditions for Fractured Coal Bodies

The state of gas transport in a coal seam is closely related to the geological structure of the seam. As the permeability in a fractured coal body is much greater than that of the original coal, it is susceptible to seepage instability, which can lead to accidents affecting mine safety. Therefore, the seepage instability process in fractured coal bodies needs to be discussed based on the theory and combined with previous test results to determine the characteristics of their seepage instability.

According to the setting of the test process, there is no acceleration of the fluid at various points in the specimen during the steady-state seepage experiment, and its flow rate is considered consistent as V. The osmotic pressure boundary body conditions can be expressed as follows:

$$\begin{cases} P\big|_{x=0} = P_1 \\ P\big|_{x=H_s} = P_2 = 0 \end{cases} \tag{6}$$

Bringing the initial and boundary conditions into the dimensionless one-dimensional non-linear kinetic equations, the expression for the system at equilibrium can be obtained as follows:

$$\begin{cases} \frac{\partial \overline{V}}{\partial x} = 0 \\ a_1 \frac{\partial \overline{P}}{\partial x} + a_2 \overline{V} + a_2 \overline{V}^2 = 0 \end{cases} \tag{7}$$

where $a_1 = \frac{P_0 \rho \beta^2 k^2}{\mu^2 c_a}$, $a_2 = \frac{\beta H_s}{c_a}$, c_a is the acceleration factor.

The total equilibrium state of the system can be simplified according to the boundary conditions of the system as follows:

$$\overline{P}(x) = \frac{P_1(1-x)}{P_0} \tag{8}$$

The speed conditions are divided into three cases, which are as follows:

- when $1 + \frac{4\rho\beta k^2 p_1}{\mu^2 H_s} < 0$, the percolation velocity after dimensionless evolution converges to negative infinity, i.e., V does not take a value;
- when $1 + \frac{4\rho\beta k^2 p_1}{\mu^2 H_s} = 0$, $\overline{V} = -\frac{1}{2}$;
- when $1 + \frac{4\rho\beta k^2 p_1}{\mu^2 H_s} > 0$;

$$\overline{V} = -\frac{1}{2} \pm \frac{1}{2}\sqrt{1 + \frac{4\rho\beta k^2 p_1}{\mu^2 H_S}} \tag{9}$$

When $\beta < 0$, satisfying $1 + \frac{4\rho\beta k^2 p_1}{\mu^2 H_s} < 0$, the motion of the characteristically non-Darcy seepage system is unstable, and the system is not in equilibrium. This means that the fractured coal body will undergo the seepage instability in this case. Therefore, the non-Darcy flow β coefficient that occurs during the test is less than zero, which can imply that the fractured coal body exhibits seepage instability. Therefore, the conditions for the occurrence of instability in the fractured coal body are as follows:

$$1 + \frac{4\beta k^2 \rho G_p}{\mu^2} < 0 \tag{10}$$

From Equation (10), the discriminant equation in the event of the seepage instability in a fractured coal body can be obtained analytically, i.e.,

$$\beta k^2 > -\frac{\mu^2 H_s}{4\rho_0 G_p} \tag{11}$$

The reason for the negative value is that the G_p value is negative, which means that when the product of the square of the non-Darcy factor and the permeability is greater than the value of the other parameters, the seepage is deemed to be unstable.

4.4.2. Analysis of Seepage Instability Parameters in Fractured Coal Bodies

This discriminant is used to judge the state of seepage at each stage, including axial displacements S of 3, 6, 9, and 12 mm, to ascertain whether seepage instability occurs at each stage. The results are summarised in Table 1.

Table 1. Permeability stability of crushed coal bodies with different grading structures.

Sample Number (Talbol Exponent)	Seepage Pressure P (MPa)	Seepage Velocity V (m/s)	Reynolds Number Calculation Re	Determination of Seepage's Loss of Stability
Group A (n = 0.2)	0.5	6.119×10^{-6}	1.688	NO
	1.0	8.304×10^{-6}	2.291	YES
	1.5	1.122×10^{-5}	3.095	YES
	2.0	1.340×10^{-5}	3.698	YES
	2.5	1.457×10^{-5}	4.020	YES
Group B (n = 0.4)	0.5	2.870×10^{-5}	2.451	YES
	1.0	3.176×10^{-5}	2.712	
	1.5	3.729×10^{-5}	3.185	
	2.0	4.210×10^{-5}	3.596	
	2.5	4.589×10^{-5}	3.919	
Group C (n = 0.6)	0.5	6.410×10^{-6}	4.895	YES
	1.0	6.847×10^{-6}	5.229	
	1.5	7.284×10^{-6}	5.563	
	2.0	7.575×10^{-6}	5.785	
	2.5	8.449×10^{-6}	6.453	
Group D (n = 0.8)	0.5	1.164×10^{-4}	1.222	NO
	1.0	1.458×10^{-4}	1.531	NO
	1.5	1.605×10^{-4}	1.685	YES
	2.0	2.082×10^{-4}	2.185	YES
	2.5	2.426×10^{-4}	2.5459	YES

The seepage instability of the percolation test is shown in detail in Table 1: as the osmotic pressure increases and the flow rate increases, the specimens are more likely to experience seepage instability. When seepage instability occurs, the instability must occur at higher osmotic pressures, whereas when the seepage instability occurs at higher osmotic pressures, it does not necessarily occur at lower osmotic pressures, i.e., a higher level of osmotic pressure is a necessary condition for the seepage instability to occur. At the same time, seepage instability occurs differently in specimens from different grades of fractured coal bodies, and there is a certain difference in the stability of specimens at different power indices n of the same osmotic pressure, indicating that there is a certain relationship between the seepage state and the gradation of the specimen. From the perspective of the Reynolds number, it is not difficult to find that the Reynolds number of different groups of specimens is greater than 1.685 when seepage instability occurs, so the relationship between the Reynolds number and seepage instability is further discussed.

The distribution of the Reynolds number for each group of specimens at different osmotic pressures can be obtained from the Reynolds number of different graded specimens at different instabilities, as shown in Figure 10.

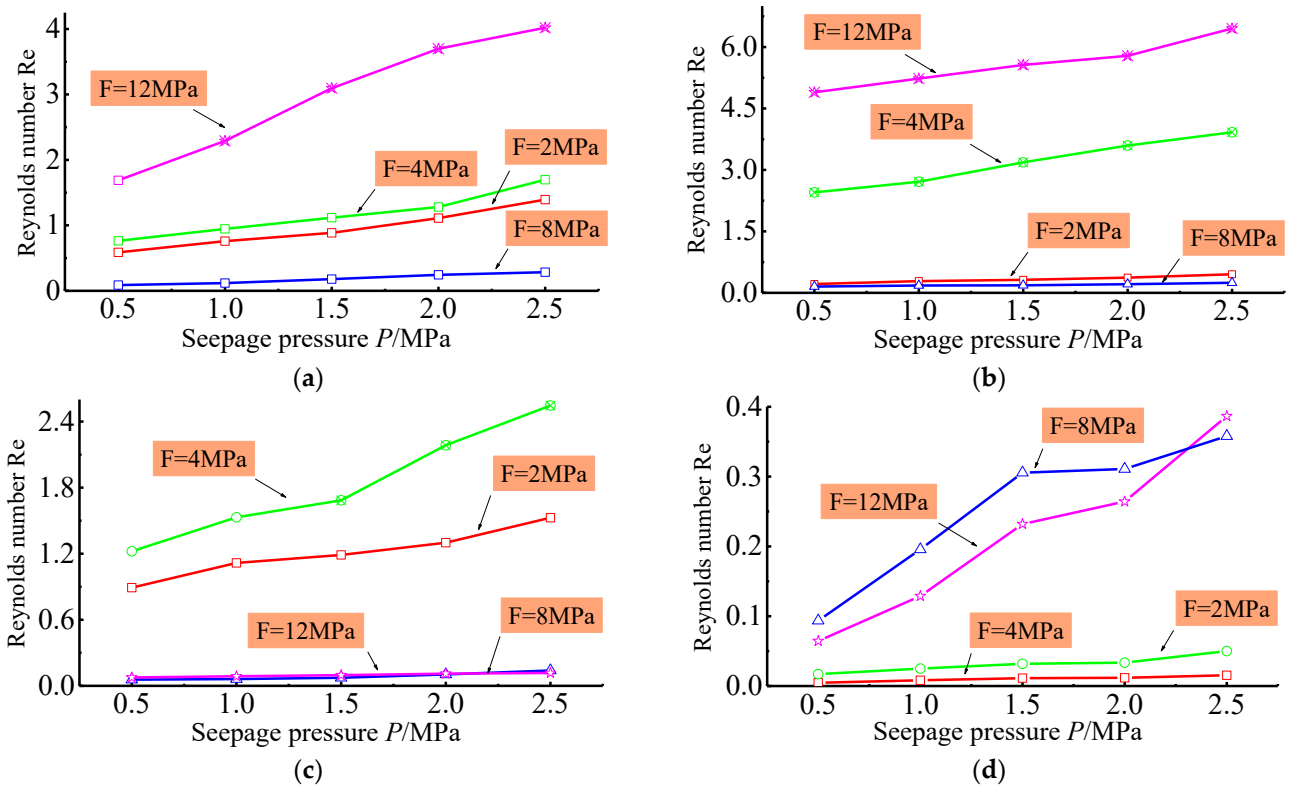

Figure 10. Reynolds number distribution at instability for each group of specimens. (**a**) n = 0.2 sets of sample; (**b**) n = 0.4 sets of sample; (**c**) n = 0.6 sets of sample; (**d**) n = 0.8 sets of sample.

As illustrated in Figure 10, when the power index n is known, with the increase in osmotic pressure, the Reynolds number at instability generally increases. Taking Figure 10a as an example, the Reynolds number of the sample at different axial displacements varies widely, and the Reynolds number of the sample at an axial displacement of 12 mm is much greater than that at other displacements. This is mainly because, as the axial displacement increases, the porosity of the sample decreases, leading to a reduction in the effective flow path of the fluid, resulting in an increase in the Reynolds number. Combining the four sets of results in Figure 10 shows that the Reynolds number increases with increasing osmotic pressure, but when the power index n is varied, there is an inconsistency in the Reynolds number at instability at different axial displacements. When the power index is taken as 0.4, 0.6, or 0.8, the Reynolds number at greater axial displacements is smaller than that at instability at lower displacements, which indicates that the variation of the Reynolds number is not only related to the axial displacement but is also related to the power index of the sample.

Generally, the Reynolds number increases with the increase in the axial displacement, but there are also cases where the axial displacement is large and the Reynolds number is small. This situation is more obvious when the power exponent n is 0.6, and the Reynolds number at the axial displacement of 12 mm is obviously smaller than that at the displacement of 3 mm. This is because the Reynolds number is related to the flow state of the fluid, and the axial displacement is not the only reason that affects the flow of the fluid inside the crushed coal body, and the permeability characteristics are determined by many common influences. The Reynolds number increases first and then decreases with the increase in the power index. When the power index n is 0.4, the Reynolds number is larger than the other groups. When the power index n is 0.8, the overall Reynolds number is smaller than that of the other groups, and infiltration and a loss of stability also occur for a small Reynolds number, which also shows that infiltration and the loss of stability are not only related to

the size of the Reynolds number but also related to the pore structure and other factors of the sample.

5. Conclusions

By measuring the permeability parameters of a crushed coal body system, the pore pressure gradient and the evolution of the system's permeability were investigated. The analysis focused on the flow distribution characteristics of the crushed coal body system and the determination method of flow sorrow, and the main conclusions obtained are drawn as follows:

- The permeation properties at different axial displacements show that the permeation properties of the crushed coal bodies obey the Forchheimer relationship, while the non-Darcian nature of the samples becomes more significant with increasing axial displacement, and the power index, which characterises the grading structure, also has an effect on the permeation of the samples. This is because as the axial displacement increases and the power index decreases, the pore structure of the sample becomes denser and the resistance of the fluid to permeation is larger, resulting in a non-linear shift in flow rate;
- The porosity of crushed coal is the main factor affecting its permeability. With the decrease in porosity, the sample's permeability k decreases and the non-Darcy factor β increases. At the same time, with the increase in n, that is, the complexity of the coal crushing degree, the permeability of the sample generally decreases, and the non-Darcy factor increases. This is because the initial internal pore structure of the samples with different grades is different, and the fracture and migration of grains during the loading process will affect the change of the final fractal structure of the samples for a while and will even lead to the penetration of the seepage channels inside the samples;
- The deformation of the permeable skeleton and the destruction of particles during the pressure-bearing process allows the pore structure to be adjusted, affecting the number and connectivity of permeable channels and the increase in resistance to the fluid, allowing a non-Darcy flow to dominate, i.e., the Forchheimer equation can better describe the state of permeability;
- Through the discussion of the stability process of the seepage loss of crushed coal, the discrimination formula of permeability k and the non-Darcy factor β was obtained. The negative non-Darcy factor is not a necessary condition for the seepage's loss of stability, but a high osmotic pressure is a necessary condition for the seepage's loss of stability. From the point of view of the Reynolds number, it is not difficult to find that the Reynolds number increases with the increase in osmotic pressure, and the increase in the gradation power index leads to the Reynolds number of the sample increasing first and then decreasing. The Reynolds number of different groups of samples is greater than 1.685 when the seepage loss is stable.

Author Contributions: M.P. contributed to the main research idea and manuscript preparation; H.P. contributed to the preparation of the manuscript and performed the correlative experiment; S.Z. and Y.Z. gave several suggestions from an industrial perspective; T.Z. assisted in finalizing the research work and manuscript. All authors have read and agreed to the published version of the manuscript.

Funding: This work was supported by the National Natural Science Foundation of China under a project entitled "Mechanism of grout diffusion behaviour and peripore fracture-porosity repair of a new liquid slow-setting sealing material" and "Mechanism of gas seepage induced by fracture extension in the 'U-shaped zone' of the double-prevention borehole" (Grant No. 52274226 and Grant No. 52104216).

Data Availability Statement: The data used to support the findings of this study are available from the corresponding author upon request.

Acknowledgments: We acknowledge the provision of the test platformed by the Key laboratory of western mine exploitation and hazard prevention of the ministry of education, whereupon tests were successfully completed and data were obtained.

Conflicts of Interest: The authors declare no conflict of interest.

References

1. Wang, G.; Shen, J.N.; Liu, S.M. Three-dimensional modeling and analysis of macro-pore structure of coal using combined X-ray CT imaging and fractal theory. *Int. J. Rock Mech. Min. Sci.* **2019**, *123*, 104082.
2. Hui, W.; Cheng, J.B.; Pz, A. Deformation and failure mechanism of surrounding rocks in crossed-roadway and its support strategy—Science Direct. *Eng. Fail. Anal.* **2020**, *116*, 104743.
3. Wang, T.; Huang, H.; Zhang, F.; Han, Y. DEM-continuum mechanics coupled modeling of slot-shaped breakout in high-porosity sandstone. *Tunn. Undergr. Space Technol.* **2020**, *98*, 103348.
4. Rahmati, H.; Nouri, A.; Chan, D. Relationship between Rock Macro-and Micro-properties and Wellbore Breakout Type. *Undergr. Space* **2019**, *6*, 62–75.
5. Chen, W. A modified model to calculate the size of the crushed zone around a blast-hole. *J. South Afr. Inst. Min. Metall.* **2016**, *116*, 485–495.
6. Yan, C.; Jiao, Y.Y.; Zheng, H. A fully coupled three-dimensional hydro-mechanical finite discrete element approach with real porous seepage for simulating 3D hydraulic fracturing. *Comput. Geotech.* **2018**, *96*, 73–89.
7. Huyakorn, P.S.; Springer, E.P.; Guvanasen, V.; Guvanasen, V.; Terry, D.W. A three-dimensional finite-element model for simulating water flow in variably saturated porous media. *Water Resour. Res.* **1986**, *22*, 1790–1808.
8. Ranjith, P. Water-weakening behavior of Hawkesbury sandstone in brittle regime. *Eng. Geol.* **2014**, *178*, 91–101.
9. Liu, K.; Ostadhassan, M. Estimation of the Permeability of Rock Samples Obtained from the Mercury Intrusion Method Using the New Fractal Method. *Fractal Fract.* **2022**, *9*, 2504–3110.
10. Ma, H.D.; Duan, J.; Zhang, X.; Liu, X.; Li, Z. Numerical simulation of water-silt inrush hazard of fault rock: A three-phase flow model. *Rock Mech. Rock Eng.* **2022**, *55*, 5163–5182.
11. Li, Q. Stability study of fluid-solid coupled dynamic system of seepage in accumulative broken rock. *Arab. J. Geosci.* **2020**, *13*, 647.
12. Dusabemariya, C.; Jiang, F.; Qian, W.; Wei, F.; Ajibola, R.B.; Romuald, A.M. Water seepage detection using resistivity method around a pumped storage power station in China. *J. Appl. Geophys.* **2021**, *188*, 104320.
13. Wu, J.; Han, G.; Feng, M.; Kong, H.; Gao, Y. Mass-loss effects on the flow behavior in broken argillaceous red sandstone with different particle-size distributions. *Comptes Rendus Mécanique* **2019**, *347*, 504–523.
14. Lv, R.S.; Zhu, Y.C.; Ma, X.Y.; Ni, X.M.; Ren, J.G. Coupled seepage mechanics model of coal containing methane based on pore structure fractal features. *Fractal Fract.* **2022**, *6*, 391.
15. Wang, Y.C.; Chen, F.; Li, X.Z.; Yin, X.; Lei, Y.T. The variable-mass seepage law of broken porous rock: An experimental study. *Geomat. Nat. Hazards Risk* **2021**, *21*, 1947–5705.
16. Liu, W.; Zhou, Y.; Chu, X. Effects of seepage behaviors on coal spontaneous combustion in longwall gobs: An investigation between Darcy and non-Darcy seepage. *Fuel* **2022**, *322*, 124126.
17. Qiu, P.T.; Chen, Z.Q.; Pu, H.; Zhu, J. Coupling effects of porosity and particle size on seepage properties of broken sandstone based on fractional flow equation. *Therm. Sci.* **2019**, *23*, 182.
18. Shi, X.; Zhou, W.; Cai, Q.; Lu, X. Experimental study on nonlinear seepage characteristics and particle size gradation effect of fractured sandstones. *Adv. Civ. Eng.* **2018**, *2018*, 8640535.
19. Liu, H.; Li, L.; Li, S.; Yang, W. The Time-Dependent Failure Mechanism of Rocks and Associated Application in Slope Engineering: An Explanation Based on Numerical Investigation. *Math. Probl. Eng.* **2020**, *2020*, 1680265.
20. Longo, A.; Pastor, M.; Sanavia, L.; Manzanal, D.; Tayyebi, S.M. A depth average SPH model including μ (I) rheology and crushing for rock avalanches. *Int. J. Numer. Anal. Methods Geomech.* **2019**, *43*, 833–857.
21. Li, X.-L.; Li, X.-L.; Wang, Y.; Peng, W.-H.; Fan, X.; Cao, Z.-Z.; Liu, R.-F. The seepage evolution mechanism of variable mass of broken rock in karst collapse column under the influence of mining stress. *Geofluids* **2023**, *2023*, 7256937.
22. Karacan, C.; Luxbacher, K. Stochastic modeling of gob gas venthole production performances in active and completed longwall panels of coal mines. *Int. J. Coal Geol.* **2010**, *84*, 125–140.
23. Kong, H.L.; Wang, L.Z.; Yin, M.G. Experimental Study on Breakage Characteristics and Energy Dissipation of the Crushed Rock Grains. *J. Civ. Eng.* **2022**, *26*, 1465–1478.
24. Sarkar, A.; Bhattacharjee, D.; Chattopadhyay, A. Size distribution of survivor clasts in pseudotachylyte and cataclasite: Implications for crushing and melting processes in seismic fault zones. *J. Earth Syst. Sci.* **2020**, *129*, 216.
25. Lei, Q. A fractal model for relative permeability in fractures under stress dependence. *Fractals* **2019**, *27*, 1950086. [CrossRef]
26. Liu, G.; Liu, L.; Liu, J.; Gao, F. A fractal approach to fully-couple coal deformation and gas flow. *Fuel* **2019**, *240*, 219–236.
27. Liu, Z.; Li, R.; Yang, H.; Zhu, D.; Taylor, T. A new fractal model of coal permeability based on the increasing fractal construction method of the MENGER sponge. *Fractals* **2021**, *29*, 2150187.
28. Xiao, B.; Li, Y.; Long, G.; Yu, B.; Taylor, T. Fractal permeability model for power-law fluids in fractured porous media with rough surfaces. *Fractals* **2022**, *30*, 1–11.

29. Pang, M.K.; Pan, H.Y.; Ji, B.N.; Zhang, H.; Zhang, T.J. Experimental investigation of flow regime transition characteristics of fractured coal bodies around gas extraction boreholes. *Energy* **2023**, *19*, 13609.
30. Li, W.; Wang, Z.C.; Qiao, L.P.; Yang, J.J.; Li, J.J. Representative elementary surface for morphology and permeability of natural rock fractures. *Bull. Eng. Geol. Environ.* **2023**, *82*, 159.
31. Tang, Y.; Wei, H.H.; Chen, Y.M.; Huang, B.; Zhang, S. Modeling of permeability for granular soils considering the particle size distribution. *Granul. Matter* **2023**, *25*, 35.
32. Jia, S.Z.; Gao, Z.G.; Yao, T.; Wang, J.K.; Gong, J.B. Fractal model-based crystal pillar structure simulation and mechanism analysis of impurity migration process in layer melt crystallization. *Chem. Eng. Sci.* **2023**, *5*, 275.
33. Qin, M.T.; Xie, S.Y.; Li, H.J.; Lou, D.; Zhang, T.F.; Carranza, E.J.M.; Kuang, Z.W. 3D Pore-Throat microstructure complexity of igneous reservoir rock and its effects on the porosity-permeability relation. *Nat. Resour. Res.* **2023**, *5*, 196.